ARTICLE

Check for updates

Phenotypic analysis of catastrophic childhood epilepsy genes

Aliesha Griffin [1,3], Colleen Carpenter[1,3], Jing Liu[1], Rosalia Paterno[1], Brian Grone[1], Kyla Hamling[1], Maia Moog[1], Matthew T. Dinday[1], Francisco Figueroa[1], Mana Anvar[1,2], Chinwendu Ononuju[2], Tony Qu[2] & Scott C. Baraban [1,2 ✉]

Genetic engineering techniques have contributed to the now widespread use of zebrafish to investigate gene function, but zebrafish-based human disease studies, and particularly for neurological disorders, are limited. Here we used CRISPR-Cas9 to generate 40 single-gene mutant zebrafish lines representing catastrophic childhood epilepsies. We evaluated larval phenotypes using electrophysiological, behavioral, neuro-anatomical, survival and pharmacological assays. Local field potential recordings (LFP) were used to screen ~3300 larvae. Phenotypes with unprovoked electrographic seizure activity (i.e., epilepsy) were identified in zebrafish lines for 8 genes; *ARX, EEF1A, GABRB3, GRIN1, PNPO, SCN1A, STRADA* and *STXBP1*. We also created an open-source database containing sequencing information, survival curves, behavioral profiles and representative electrophysiology data. We offer all zebrafish lines as a resource to the neuroscience community and envision them as a starting point for further functional analysis and/or identification of new therapies.

[1] Epilepsy Research Laboratory and Weill Institute for Neuroscience, Department of Neurological Surgery, University of California San Francisco, San Francisco, CA, USA. [2] Helen Wills Neuroscience Institute, University of California, Berkeley, CA, USA. [3] These authors contributed equally: Aliesha Griffin, Colleen Carpenter. ✉email: scott.baraban@ucsf.edu

Catastrophic childhood epilepsies are characterized by intractable persistent seizures and are frequently associated with developmental delay, cognitive dysfunction, and autism[1–3]. Many are rare genetic disorders lacking effective therapeutic options[4–6]. With technological advances and large-scale patient cohorts, genome-wide analyses have now identified de novo mutation in a single gene for most of these epilepsies[7–11]. These studies highlight the complexity of epilepsy, as mutations in genes coding for ion channels, ligand-gated receptors, solute transporters, metabolic enzymes, synaptic trafficking proteins, kinases, transcription factors, and adhesion molecules were identified. Unfortunately, our overall understanding of genetic epilepsies is severely limited as few experimental animal models exist, and human-induced pluripotent stem cell-derived two- or three-dimensional neuronal models fail to fully recapitulate the complex brain network seen in patients. Zebrafish, a small vertebrate with considerable genetic similarity to humans[12], offer an attractive alternative model to study these genetic mutations in vivo. Analysis of zebrafish mutants for human genes has provided valuable insight into complex circuits controlling behavior[13–17], evolutionarily conserved developmental programs[18–20], and drug candidates for a variety of diseases, including epilepsy[21–29].

Epilepsy classification, incorporating an understanding of different seizure types and comorbidities, is an essential clinical resource in evaluating patients and selection of antiseizure treatments[30–33]. Seizure classifications promoted by the International League Against Epilepsy (ILAE)[33] are largely defined by the presence of unprovoked "self-sustained paroxysmal disorders of brain function" and these classification resources have evolved continuously since the 1960s. However, adaptation of this strategy to animal models[34], specifically zebrafish models developed for catastrophic epilepsies of childhood, is difficult. Because electrophysiological monitoring is a critical component of clinical diagnosis, we primarily focused our phenotyping effort on describing the full spectrum of electrical events encountered. Such an electrophysiology database, broadly adapted, could be particularly useful for preclinical studies designed to characterize epilepsy phenotypes in any larval zebrafish model.

To better understand mechanisms underlying human genetic epilepsies, it is important to first identify clinically relevant phenotypes in an experimental model system[35]. Although efficient gene inactivation in mice contributed pediatric epilepsy models[36–38], to generate dozens of mutant mouse lines followed by a systematic phenotypic analysis would require several decades of research. Using an efficient CRISPR-based gene editing strategy[39,40] we successfully generated 37 stable zebrafish lines representing human monogenic pediatric epilepsies. Large-scale phenotypic analysis of survival, behavior, and electrographic brain activity was performed. We established readouts to identify seizures at electrographic and behavioral levels, and an open-source online website to efficiently share data with the neuroscience community. As many of these zebrafish represent rare genetic diseases for which our understanding of pathophysiology remains largely unknown, they provide a rich resource to further investigate key etiological questions or utilization in high-throughput precision medicine-based therapy development.

Results
Generation of loss-of-function models for human epilepsy genes.
We evaluated genes identified in humans using genome-wide association (GWAS) and pathological de novo variants from trio exome sequencing studies[6–10,41]. First, analysis of human genetic data was performed to identify genes where a loss-of-function (LOF) mutation was likely a causal mechanism of the epileptic phenotype. This limited our initial Epilepsy Zebrafish

Project (EZP) choices to 63 gene candidates (Supplementary Table 1). Second, Epilepsy Genetics Initiative identified human genes were selected representing 57 orthologous zebrafish genes (Fig. 1a). From this group, we identified 48 zebrafish genes that were high confidence orthologs (Fig. 1b, homology scores; Supplementary Table 2) and examined expression data patterns with a primary focus on brain expression (Fig. 1c). Third, RT-PCR confirmed gene expression for 46 zebrafish orthologs from the four-cell to 7 dpf stage (Fig. 1e) e.g., an early neurodevelopmental window wherein high-throughput studies would be feasible. To generate stable mutant lines, we used Cas9 with a single in vitro transcribed guide RNA (with no predicted off-target sites) targeted towards the start of the protein-coding sequence. A total of 46 zebrafish orthologous genes were targeted (Supplementary Table 3). This group includes a previously published stxbp1b mutant[42] and a scn1lab CRISPR mutant. Adult founders harboring predicted protein-coding deletions (Fig. 1e; https://zebrafishproject.ucsf.edu) were confirmed and outcrossed for at least two generations. All EZP zebrafish were maintained as outcrossed lines with phenotypic assessment(s) performed on larvae generated from a heterozygous in-cross. For seven genes we could not obtain a viable line (grin2aa, syngap1a, tbc1d24, prickl1a, plcb1, gosr2, and stx1b). In total, 37 EZP zebrafish lines were subjected to phenotypic screening described below.

Electrophysiological screening of larval zebrafish.
We previously described minimally invasive local field potential recording (LFP) techniques to monitor brain activity in larval zebrafish[43] (Supplementary Fig. 1). To identify epilepsy phenotypes in CRISPR-generated zebrafish lines, we obtained LFP recordings from 3255 larvae at 5 and 6 day post fertilization (dpf). We blindly recorded a minimum of 75 larvae per line, from at least three independent clutches. Larvae were randomly selected and genotyped post hoc to evaluate homozygote, heterozygote, and wild-type (WT) phenotype-genotype correlations. Although long-duration, multi-spike large-amplitude discharges are commonly described as seizure events in larval zebrafish models[23,44–48], the full spectrum of potential electrical activity is unknown. An LFP electrophysiology-based scoring system covering all types of observed activity was established: (i) type 0: the range of low voltage activities and patterns of small membrane fluctuations; (ii) type I: low amplitude interictal-like sharp waveforms, with voltage deflections at least three times above baseline (duration range: 10–99 msec); and (iii) type II: large amplitude ictal-like multi-spike waveforms, with voltage deflections at least five times above baseline (duration range: 45–5090 msec), often followed by a transient period of electrical suppression with no detectable events (Fig. 2a). Based on this numeric scoring system, each 15 min recording epoch was assigned an LFP score by two independent investigators; cumulative averages can be seen in the heatmap for all 37 EZP-generated zebrafish lines (Fig. 2b). We classified mutants with an average LFP score of 1.0 or above as epilepsy phenotype. These included two genes previously determined to exhibit epilepsy phenotypes in zebrafish (e.g., scn1lab[23] and stxbp1b homozygotes[42]) and six novel zebrafish epilepsy lines (e.g., arxa, eef1a2, gabrb3, pnpo, strada homozygotes, and grin1b heterozygotes). The percentage of EZP mutant larvae scored at type II ranged from 29 to 83% for epilepsy lines and a significant correlation between LFP scores versus the percentage of type II mutants was noted (Fig. 2c; $R^2 = 0.8790$). Distribution of LFP scores for all WT larvae skewed toward type 0 (mean WT score = 0.66; $n = 781$) and was significantly different than scoring distributions for mutant lines designated as epileptic (mean EZP epilepsy score = 1.23; $n = 190$; unpaired t test $p < 0.0001$, $t = 10.26$, $df = 969$)
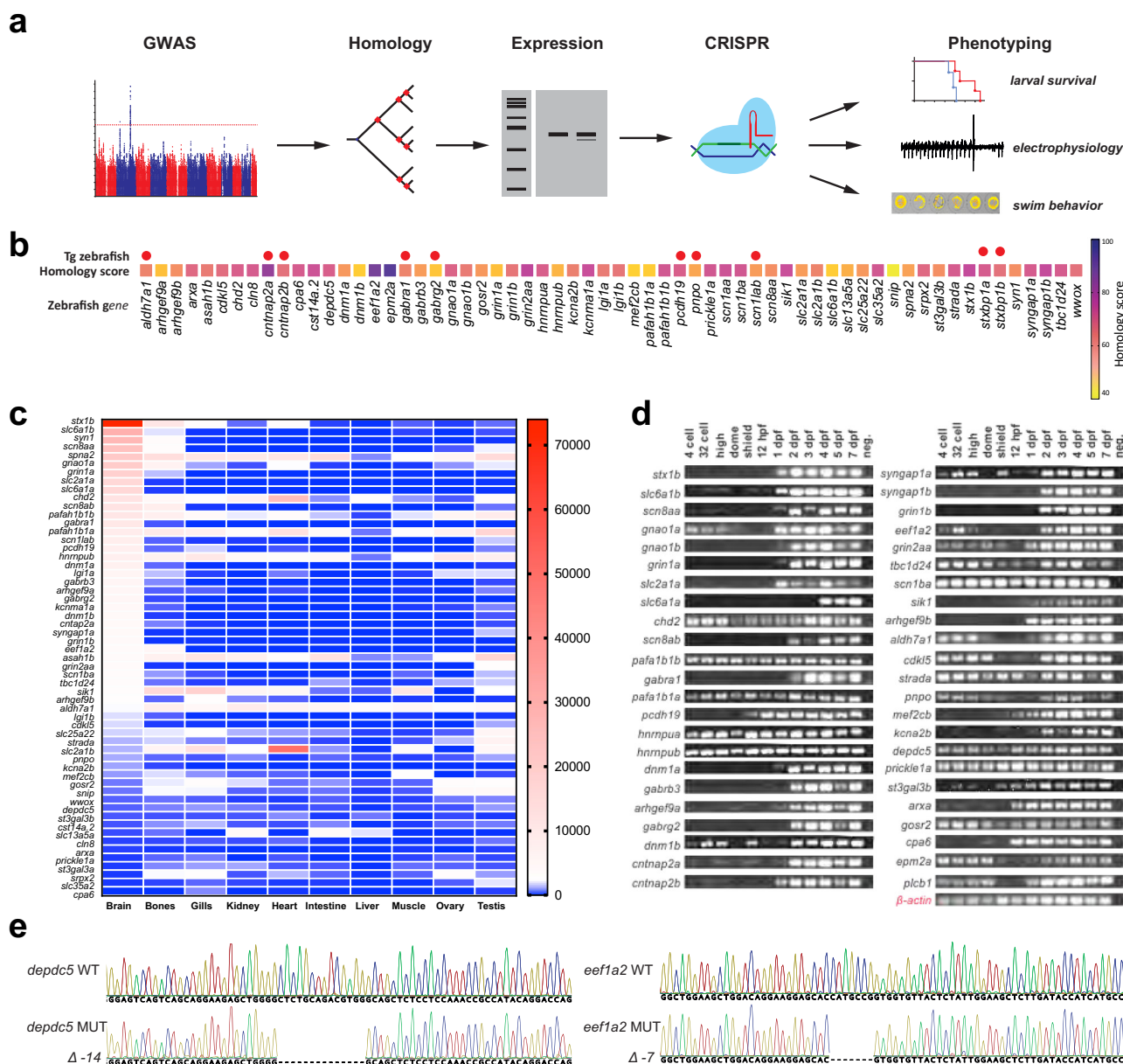
Fig. 1 The Epilepsy Zebrafish Project (EZP). a Overview of the zebrafish epilepsy disease model discovery workflow from human genome-wide association studies (GWAS) to the generation of zebrafish models and phenotypic characterization. **b** Heatmap of homology scoring for all EZP zebrafish lines generated. Red circles indicate genes for which mutant zebrafish lines were previously published. **c** Tissue expression profiles of EZP zebrafish target genes. Heatmap represents the maximum number of sequence reads for each gene per tissue. **d** Developmental gene expression profiles for EZP lines. **e** Representative frame-shift mutant lines confirmed for *depdc5* and *eef1a2*.

(Fig. 2d). The majority of LFP recordings from all lines were classified as type 0 or 1 (79%; $n = 3255$; Fig. 2e).

We next examined the frequencies, durations, and spectral features of spontaneous epileptiform events recorded in all eight EZP epilepsy lines. To provide an unbiased quantitative analysis, type I interictal- and type II ictal-like electrical events were detected using custom software (see Methods; Fig. 3) on homozygote and WT sibling larvae recordings. Representative LFP recordings (Fig. 4b, top) with accompanying time-frequency spectrograms (Fig. 4b, bottom) are shown for each EZP epilepsy line; individual LFP scoring distribution plots for mutants and WT siblings are shown at left. No difference in interictal-like (type I) event frequency or duration was noted (Fig. 4c). Ictal (type II) events were more frequent and longer in duration for *scn1lab* mutant compared with WT; ictal event duration was

shorter for *stxbp1b* mutants compared with WT (Fig. 4d). Ictal event histograms showed similar overall distributions at a cumulative and individual level (Fig. 5; Supplementary Figure 2). However, large-amplitude multi-spike ictal events when present in WT siblings were usually brief in duration, rarely exceeding 2.0 s (Figs. 5a, c) and less frequently encountered (Fig. 5b) than those identified in EZP epilepsy lines (also see cumulative distribution insets in Supplementary Figure 2a). Representative raw LFP traces and scoring distribution plots for all 37 zebrafish lines can be explored on our open-source website, https://zebrafishproject.ucsf.edu, where users can also find information on homology, sequencing, survival, and genotyping protocols.

EZP lines for understanding disease pathophysiology. Epileptic zebrafish can be used to study underlying neurobiological
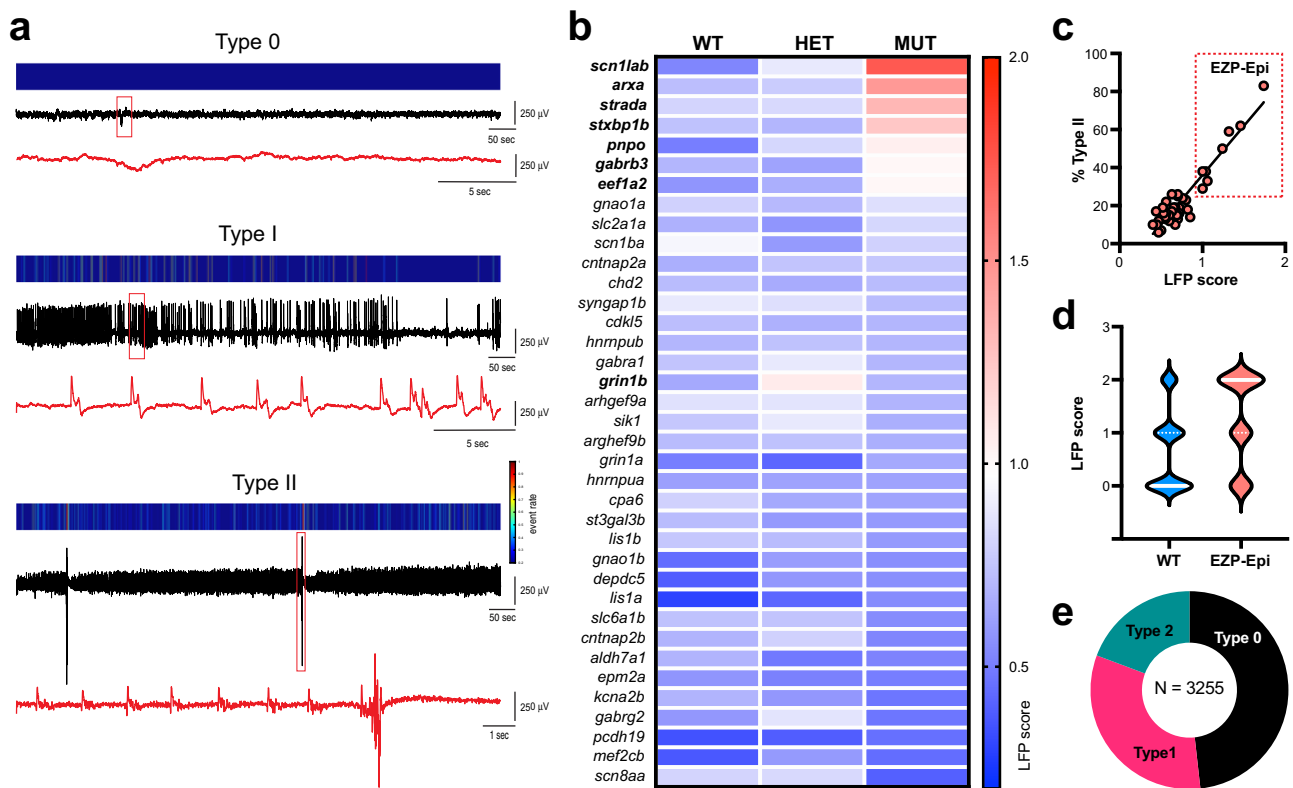
Fig. 2 Electrophysiological screening of EZP lines. a LFP recordings representing type 0 (low voltage, small, or no membrane fluctuations), type I (low amplitude, sharp interictal-like waveforms), and type II (low frequency, sharp ictal-like waveforms with large-amplitude multi-spike events and post-ictal slowing) scoring activity. For each example, a color-coded event rate histogram, full 15 min LFP recording, and high-resolution LFP close-up (red box, red trace a) are shown. **b** Heatmap showing mean larval zebrafish LFP recording scores for all 37 EZP zebrafish lines ranked from highest homozygote score to lowest; $N = 77–127$ larvae per gene (see https://zebrafishproject.ucsf.edu for N values on each individual line). A threshold of a mean LFP score >1.0 was classified as an EZP line exhibiting epilepsy (indicated in bold font: scn1lab, arxa, strada, stxbp1b, pnpo, gabrb3, eef1a2, and grin1b). **c** Regression plot for all 37 mutants showing mean LFP score versus % of Type II larvae for each homozygote. Seven homozygote and one heterozygote lines highlighted in "EZP-epi" box as clearly differentiated from a cluster of 31 non-epileptic EZP lines with LFP scores <1.0. Simple linear regression $R^2 = 0.8790$; ***Significant deviation from zero, $p < 0.0001$; DFn, DFd = 1, 36. **d** Violin plots of all LFP scores recorded for EZP epilepsy lines ($N = 190$) compared with all WT control siblings ($N = 783$ larvae). Note: type 2 epileptiform events were only observed in 14.7% of all WT larvae. **e** Distribution of Type 0, I, and II scores for all WT, heterozygote, and homozygote larvae screened by LFP recordings ($N = 3255$ larvae).

mechanisms, behavioral comorbidities, and drug discovery. Many pediatric epilepsies are associated with increased mortality rates and thus, survival studies were performed on all EZP lines to evaluate larval health, confirm Mendelian genotyping ratios, and identify early death phenotypes (Fig. 6a, Supplementary Figure 3). Early fatality was noted in aldh7a1, depdc5, scn8aa, and strada homozygous mutants that only survive between 8 and 10 dpf (Fig. 6b).

We further performed a series of pilot experiments in all eight EZP-epileptic lines to investigate other known pathophysiology. Epilepsy often manifests as convulsive behaviors in many of these genetic epilepsies. Prior work from our laboratory using chemically induced (pentylenetetrazole; PTZ) or an ENU-mutagenesis mutant for Dravet syndrome ($scn1lab^{s552/s552}$) describes a characteristic series of larval seizure-like behaviors, culminating in bursts of high-speed swim activity and whole-body convulsions[23,44]. Using these well-established models, we first developed a custom MATLAB algorithm to detect high-speed (≥ 28 mm/s), long-duration (≥ 1 s) behavioral events corresponding to these convulsive behaviors in freely behaving larvae (Fig. 7). The MATLAB-detected behavioral event duration was similar to that measured for type II ictal-like events in LFP recordings (see Fig. 5). As expected, EZP-generated scn1lab mutant larvae displayed significantly higher velocity movements and higher frequencies of convulsive-like events compared with

WT sibling controls; similar results were obtained with $scn1lab^{s552/s552}$ larvae. There was no difference in the total distance traveled between WT and homozygous mutants in these lines (Fig. 6c). Maximum velocity and total distance measurements show that arxa larvae are hypoactive and they had no detectable high-speed, long-duration events during these 15 min recording epochs (Fig. 6c; Fig. 6d, representative traces). We observed that the duration of high-speed events in $scn1lab^{s552/s552}$ larvae were significantly longer than in WT sibling controls (Fig. 6e). No significant behavioral phenotypes were seen in the other epileptic lines (Supplementary Figure 4).

ARX-related epilepsies are categorized as "interneuronopathies"[49] and Arx mutant mice exhibit a reduced number of interneurons in both neocortex and hippocampus[50,51]. Using volumetric light-sheet microscopy imaging in larval arxa mutants co-expressing a green fluorescent protein (GFP) in Dlx-labeled interneurons[52], we confirmed a significant reduction in interneuron density for homozygous arxa mutant larvae compared with WT sibling controls (Fig. 8a). EEF1A2 mutations are associated with neurodevelopmental deficits in some patients[53]. Using conventional morphological analyses measuring overall head length, midbrain/forebrain width, and body length on in vivo images from eef1a2 mutant larvae and WT siblings at 5 dpf, we noted no differences (Fig. 8b). Patients with GABRB3 mutations, like many of the genes studied here, are often classified as pharmaco-resistant[54]. Using a
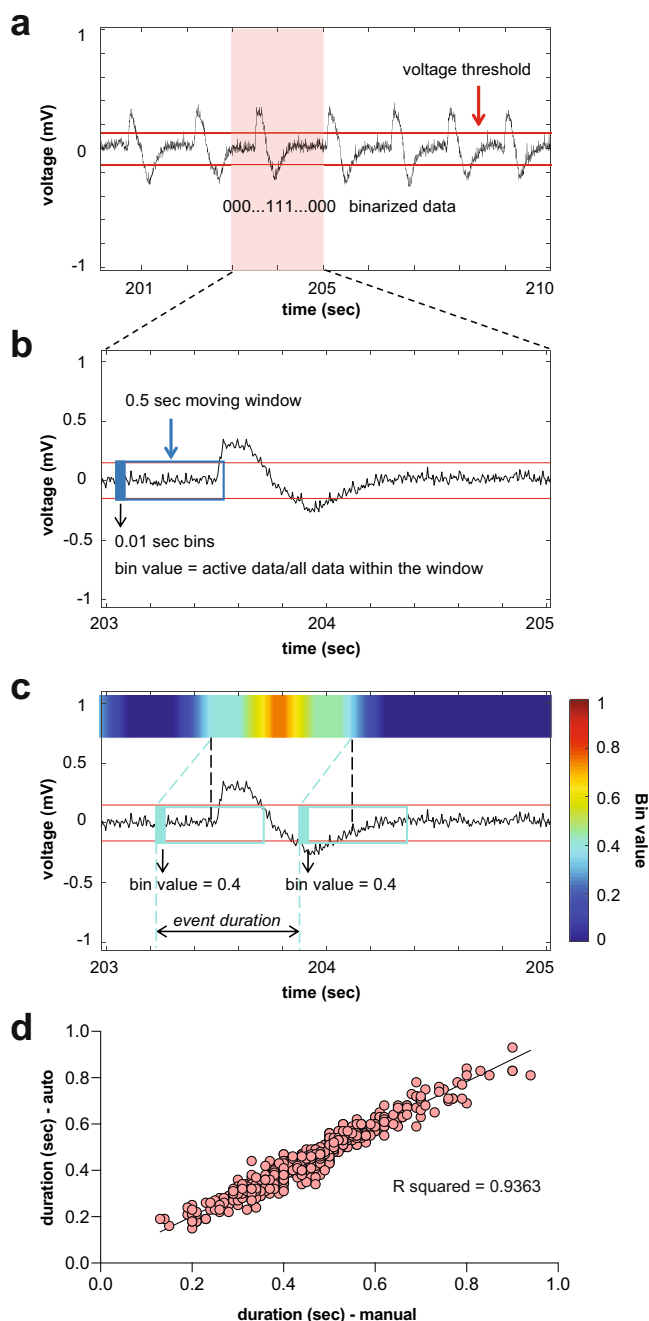
Fig. 3 Automated interictal-like event quantification. a A representative LFP recording with interictal-like events. A voltage threshold (0.15–0.25 mV, depending on the noise level) was set for event detection. Data were binarized by threshold: super-threshold data points were scored as 1, and under-threshold data points were scored as 0. **b** A data binning method was used for automated quantification of interictal-like events: 0.01 s binning in 0.5 s time window. In each window, the value of the first bin was calculated, which is the ratio of active data points to the number of total data points within the window. **c** Color raster plots were created according to the raster score. A raster score threshold (0.2–0.4) was set to define the start and end of an event. **d** Comparison between interictal-like event durations measured automatically and manually. A 10 s representative epoch from each recording will be used as a testing sample to optimize the algorithm. Voltage and raster score thresholds were chosen when the difference between automated and manual results is <3% of manual measurements.

1 hr LFP recording protocol, we evaluated electrographic seizure activity in *gabrb3* mutants treated with standard antiseizure drugs: carbamazepine, valproate, and topiramate. In these zebrafish mutants, carbamazepine suppressed high-frequency interictal-like and long-duration multi-spike ictal-like epileptiform discharges (Fig. 8c). Patients with *ALDH7A1* mutations are associated with pyridoxine-dependent encephalopathy. Using a CRISPR-generated *aldh7a1ot100* mutant, Pena et al.[46] reported hyperactive behavior and spontaneous electrographic seizures starting at 10 dpf; 10 mM pyridoxine treatment rescued these phenotypes. The unperturbed EZP-generated *aldh7a1* mutant larvae die prematurely between 7 and 9 dpf. Daily 10 mM pyridoxine effectively extended the median survival of *aldh7a1* mutant larvae to that observed in heterozygote and WT sibling controls (Fig. 8d).

Discussion

Progress in exploring pathogenesis, and developing new therapies, for monogenic epilepsies is complicated by the limited availability of preclinical animal models for many of these genes. The emergence of zebrafish as a vertebrate model system amenable to genetic manipulation holds much promise toward accelerating progress in understanding these rare epilepsies. Here, we utilized CRISPR/Cas9 and a battery of larval zebrafish assays to systematically evaluate 40 different single-gene mutations identified in this population. We determined that homozygous deletion of *arxa*, *eef1a2*, *gabrb3*, *pnpo*, *scn1lab*, *strada*, and *stxbp1b* or heterozygous loss of *grin1b* result in recurrent unprovoked electrographic seizures (i.e., epilepsy). In addition, we developed the first version of an electrophysiology-based scoring system that can be used to identify seizure-like activity in any larval zebrafish model. Finally, we show that clinically relevant phenotypes such as interneuron loss (*arxa*) or pharmaco-resistance (*gabrb3*) can be recapitulated in zebrafish models.

Although CRISPR/Cas9 works with remarkable efficiency to disrupt gene function in zebrafish[39,40], recent large-scale efforts have not reported on epilepsy or clinically relevant functional outcome measures[16,17]. To present robust and well-controlled functional assays, we outcrossed all EZP lines a minimum of three generations and blindly analyzed homozygous, heterozygous, and WT siblings. This approach avoids off-target or toxicity effects from microinjection of CRISPR/Cas9 editing that might cause identification of false positives. A limitation typical of these types of CRISPR-based larval zebrafish studies, focused primarily on novel genes, is that the full spectrum of tools (antibodies, etc.) or functional assays (single-cell electrophysiology) necessary to confirm LOF mutation are not available. Nonetheless, epileptic activities seen in CRISPR/Cas9 deficient (*aldh7a1*)[46,55] or ENU-generated (*scn1lab*s552/s552)[23] zebrafish were successfully recapitulated here. Interestingly, but perhaps not surprisingly, the majority of our CRISPR-generated single gene LOF zebrafish mutants were not associated with epilepsy phenotypes at this stage of larval development (5–6 dpf). It is possible that many of these single-gene mutations are one factor in the emergence of epilepsy in humans, but full clinical phenotypes rely upon polygenic factors[56,57], epigenetics[53], or environmental issues such as early-life febrile seizures[58]. Developmental considerations are an additional confounding factor[2,3], as clear epileptic phenotypes may emerge at later juvenile or adult timepoints. Although a potential limitation for interpretation of these studies, we chose to focus this initial phenotypic screening effort on larval developmental ages that would lend themselves to future high-throughput drug discovery. Where single-gene mutant mice are available for electrophysiology comparisons a similar lack of
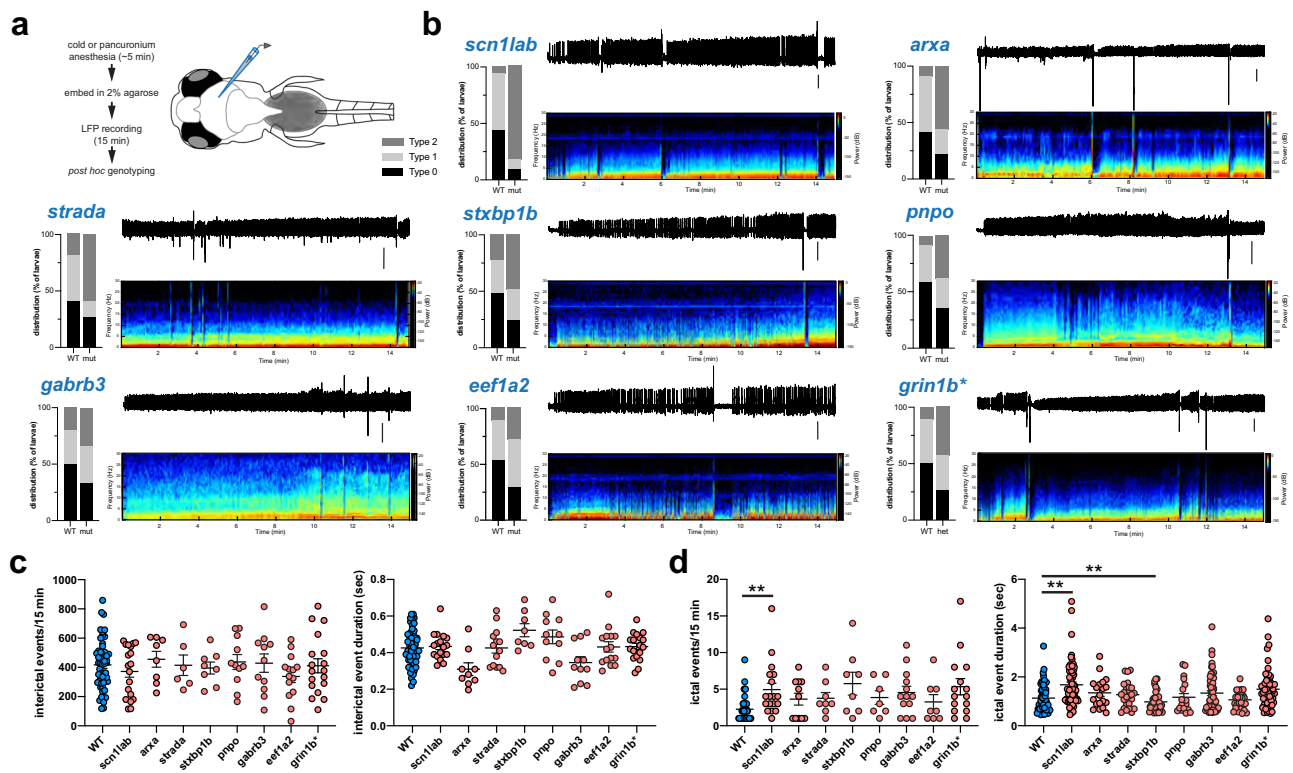
Fig. 4 Electrographic seizure activity in epileptic zebrafish mutant lines. a Schematic of recording configuration and protocol for electrophysiology-based screening of larval zebrafish. **b** Representative raw LFP-recording traces along with a corresponding wavelet time-frequency spectrogram and LFP scoring distribution plot for WT and mutant larvae are shown for each EZP epilepsy line. Type 0, I, and II scoring as in Fig. 2. A representative WT LFP recording with the corresponding wavelet time-frequency spectrogram is shown in Supplementary Figure 5. Scale bar = 500 μV. Representative LFP recordings and distribution plots for all 37 lines can be found online (https://zebrafishproject.ucsf.edu). **c** Cumulative plots of interictal event frequency and duration for all EZP epilepsy lines compared with WT sibling controls. Each point represents mean of all interictal events in a single 15 min larval LFP recording detected using custom software in MATLAB (N = 9775, WT; N = 6750, scn1lab; N = 2550, arxa; N = 5790, strada; N = 6750, stxbp1b; N = 3538, pnpo; N = 3455, gabrb3; N = 4335, eef1a2; N = 6610, grin1b*). **d** Cumulative plots of ictal event frequency and duration. Each point represents all ictal events in a single 15 min larval LFP recording (N = 56, WT; N = 62, scn1lab; N = 26, arxa; N = 26, strada; N = 48, stxbp1b; N = 22, pnpo; N = 59, gabrb3; N = 27, eef1a2; N = 55, grin1b*). *for grin1b designates heterozygote. **p < 0.01, ANOVA with Dunnett's multiple comparisons test. Data displayed as mean ± SEM.

unprovoked seizure phenotypes (i.e., epilepsy) have been reported e.g., Cdkl5[59,60], Chd2[61], or Depdc5[62]. Further, the frequency and severity of seizure activity in patients with single-gene mutations can also be variable, e.g., SCN8[63], PCDH19[64], MEF2C[65], CDKL5, and ARX[66], which highlights the complexity of modeling rare epilepsy gene candidates.

Our previous studies established the presence of hyperactive and seizure-like (stage III) behaviors in PTZ-treated WT larvae and spontaneously in scn1lab[s552/s552] mutant larvae, a model of Dravet syndrome[23,44]. These stage III behaviors are defined as brief clonus-like convulsions followed by a loss of posture, where a larva falls on its side and remains immobile for 1–3 s (manually scored)[44]. Behavioral readouts were instrumental in primary screens aimed at finding anti-epileptic drugs that treat Dravet syndrome, ultimately allowing us to test over 3500 drugs in <5 years[23,24,27] and advancing our lead candidate to clinical trials (https://clinicaltrials.gov/ct2/show/NCT04462770). Here, we further refine our definition of seizure-like movements as events ≥28 mm/s in velocity and ≥1 s in duration and created a MATLAB algorithm to efficiently detect these events in behavioral assays; total distance moved was not a reliable measure of these events. Spontaneous large-amplitude LFP events, categorized as type 2, appear to correspond in duration to behavioral seizure-like convulsive movements and potentially represent a zebrafish form of ictal epileptiform activity; high-frequency small-amplitude events, categorized as Type 1, could

represent a less-severe interictal-like abnormality or possibly a normal variant of activity. Interestingly, of our eight EZP epilepsy CRISPR lines, only the most robust phenotypic line (scn1lab mutants; see Fig. 1b) had significantly more seizure-like behavioral events compared to controls, suggesting that hyper-locomotion alone may not be sufficient to identify epileptic phenotypes. Interestingly, hypo-locomotion seen here in arxa mutant larvae [also reported in tsc2[67] and gabrg2[68] mutants, respectively] may represent a pathological behavioral state. Ultimately and mimicking clinical diagnoses of epilepsies using video-electroencephalographic monitoring[2,30,44], our electrophysiology-based screening approach successfully identified spontaneous epileptiform activity that was not easily detected in locomotion-based assays. Although simple locomotor readouts have grown popular as seizure assays[69–74], this study emphasizes the scientific rigor necessary to accurately identify epileptic phenotypes in zebrafish and suggests that sole reliance on simple behavioral readouts may lead to misleading conclusions during phenotyping and/or drug discovery efforts.

Conclusion

Overall, the EZP demonstrates the power of large-scale phenotype-based analyses of human gene mutations and all mutant lines are available to the scientific community (https://zebrafishproject.ucsf.edu). These CRISPR-generated zebrafish
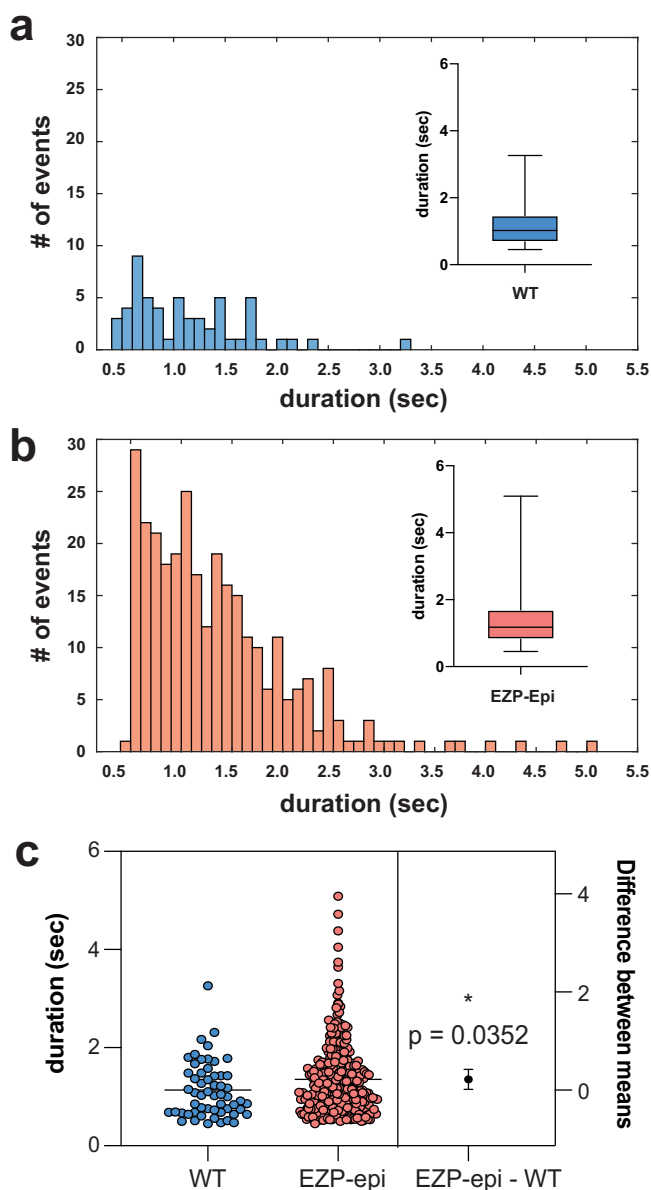
Fig. 5 Distribution of ictal-like events. Histograms depict number and duration of ictal events measured using a custom MATLAB-based program for **a** all sibling wild-type (WT) larvae from EZP epilepsy lines and **b** same for epileptic zebrafish lines (EZP)-Epi. Box-and-whisker plots showing the distribution of ictal event durations; mean and minimum/maximum values are shown (insets). **c** Estimation plot showing that ictal event duration for WT (1.134 ± 0.075 s; $N = 56$ larvae) is shorter than for Epi-EZP (1.353 ± 0.043 s; $N = 299$ larvae); Non-parametric t test *$p = 0.0352$, $t = 2.115$, $df = 353$). Each dot on the top plot represents the duration (measured in msec) for one individual ictal event. LFP recording epochs were 15 min. Data displayed as mean ± SEM.

models have two important advantages: first, they provide a valuable in vivo model system to explore underlying pathophysiological mechanisms in rare genetic epilepsies. Second, they provide an easily accessible preclinical model system for high-throughput drug discovery and therapy development that is far more efficient than rodent models. The spectrum of electrographic activity observed and pilot neurodevelopmental/pharmacological data were provided for several epileptic zebrafish lines here as a potential starting point for further investigations. We anticipate, and hope, that future studies using these zebrafish

will help us to better understand genetic disorders and further the ultimate vision of precision medicine.

Methods

Zebrafish husbandry. All procedures described herein were performed in accordance with the Guide for the Care and Use of Animals (ebrary Inc., 2011) and adhered to guidelines approved by the University of California, San Francisco Institution Animal Care and Use Committee (IACUC approval #: AN171512-03A). The zebrafish lines were maintained in a temperature-controlled facility on a 14:10 hour light:dark cycle (9:00 AM to 11:00 PM PST). Juvenile and adult zebrafish were housed on aquatic units with an automated feedback control unit that maintained the system water conditions within the following ranges: temperature; 28–30 °C, pH; 7.5–8.0, and conductivity; 690–740 mS/cm. Juveniles (30–60 dpf) were fed twice daily, once with JBL powder (JBL NovoTom Artemia) and the other with JBL powder + live brine shrimp (Argent Aquaculture). Older juveniles and adults were also fed two times per day, first with flake food (tropical flakes, Tetramin) and then with flake food and live brine shrimp. At larval stages used here, zebrafish have not yet experienced sexual differentiation. Zebrafish embryos and larvae were raised in an incubator kept at 28.5 °C under the same light–dark cycle as the facility. The solution or "embryo medium" used for the embryos and larvae consisted of 0.03% Instant Ocean (Aquarium Systems, Inc.) and 0.000002% methylene blue in reverse osmosis-distilled water. Larvae were fed with powder (6–10 dpf) or JBL powder + brine shrimp (11–29 dpf).

Zebrafish homology prediction. To improve our confidence in modeling epilepsy at the genetic level in zebrafish, we established a zebrafish homology score. To determine the homology score the percent protein identity and DIOPT score were used. The percent protein identity was established from Ensembl (GRCz10) using the predicted human orthologue gene. When the human orthologue gene was not predicted by Ensembl, a Clustal Omega analysis was performed using standard parameters. The DIOPT score was established using the MARRVEL (http://marrvel.org/) database and is the number of orthologue prediction tools that predicted a given orthologue pair. Twelve orthologue prediction tools (Comara, Eggnog, Homologene, Inparanoid, OMA, OrthoDB, orthoMCL, Panther, Phylome, RoundUP, TreeFam, and ZFIN) were used to predict zebrafish orthologs. The homology score represents the average of the percent identity and the DICOT score as a percentage. A gene with a homology score >65 was considered for the EZP.

Zebrafish gene expression analysis. Adult tissue expression was determined using the Phylofish database[75]. Development expression was determined using semi-quantitative RT-PCR. Pools of 25–50 zebrafish embryos or larvae were collected at 4-cell, 32-cell, high, sphere, 12 hpf, 1, 2, 3, 4, 5, and 7 dpf for expression analysis. Total mRNA was extracted from whole embryos or larvae using a phenol/chloroform extraction protocol. After extraction, 1 μg of purified RNA was treated with DNaseI and retrotranscribed to cDNA using the following SuperScript IV Reverse Transcriptase (8091050, Invitrogen) the manufacturer's protocol. The temporal expression of genes was characterized RT-PCR using GoTaq Master Mix (M712C, Promega) and oligonucleotide sequences are listed at https://zebrafishproject.ucsf.edu. Thermal cycling conditions included an initial denaturation at 95 °C for 5 min, followed by 40 cycles at 95 °C for 30 s, 56 °C for 30 s, and 72 °C for 30 s and a final incubation at 72 °C for 7 min.

Generation of CRISPR mutant lines. Zebrafish mutant lines of the 40 genes were generated using CRISPR-Cas gene editing in Tupfel Long-Fin (TL) wild-type zebrafish (ZIRC). CRISPRscan was used to identify sgRNA sequences with high predicted cut efficiencies for early exons and sgRNAs were synthesized using T7 in vitro transcription with the MEGAshortscriptTM T7 Transcription Kit (AM1354, ThermoFisher). To minimize off-target effects, we selected target sites with the lowest number of potential mutagenesis and with a minimum of three mismatches with every other site in the genome. Fertilized embryos (1–2 cell stage) were co-injected with ~2 nl of sequence-specific sgRNA (~10–25 ng/μl), Cas9 mRNA (~250 ng/μl), and 0.4% rhodamine b. At one dpf, embryos were sorted for fluorescence and genomic DNA extracted using Zebrafish Quick Genotyping DNA Preparation Kit (GT02-02, Bioland Scientific) from pools of 5–10 healthy, microinjected, and un-injected larvae. The samples were Sanger sequenced to assess gene editing at the guide target site. Once editing was confirmed, the remaining embryos were raised to adulthood. Resulting F0 mosaic adults, confirmed by Sanger sequencing DNA from fin-clips, were crossed with TL zebrafish to create stable heterozygote F2 and greater generations of breeders for our experiments. Guide RNA, primer sequences, and PCR protocols for all lines can be found in Supplementary Table 3. All experiments were done blinded using unfed larvae between 3 and 14 dpf. At this stage, larvae are sexually indistinguishable.

Electrophysiology. Zebrafish larvae (5–6 dpf) were randomly selected, exposed to cold anesthesia or pancuronium (300 μM), and immobilized, dorsal side up, in 2% low melting point agarose (BP1360-100, Fisher Scientific) within a vertical slice perfusion chamber (Siskiyou Corporation, #PC-V). Slice chambers containing one or two larvae were placed on the stage of an upright microscope (Olympus
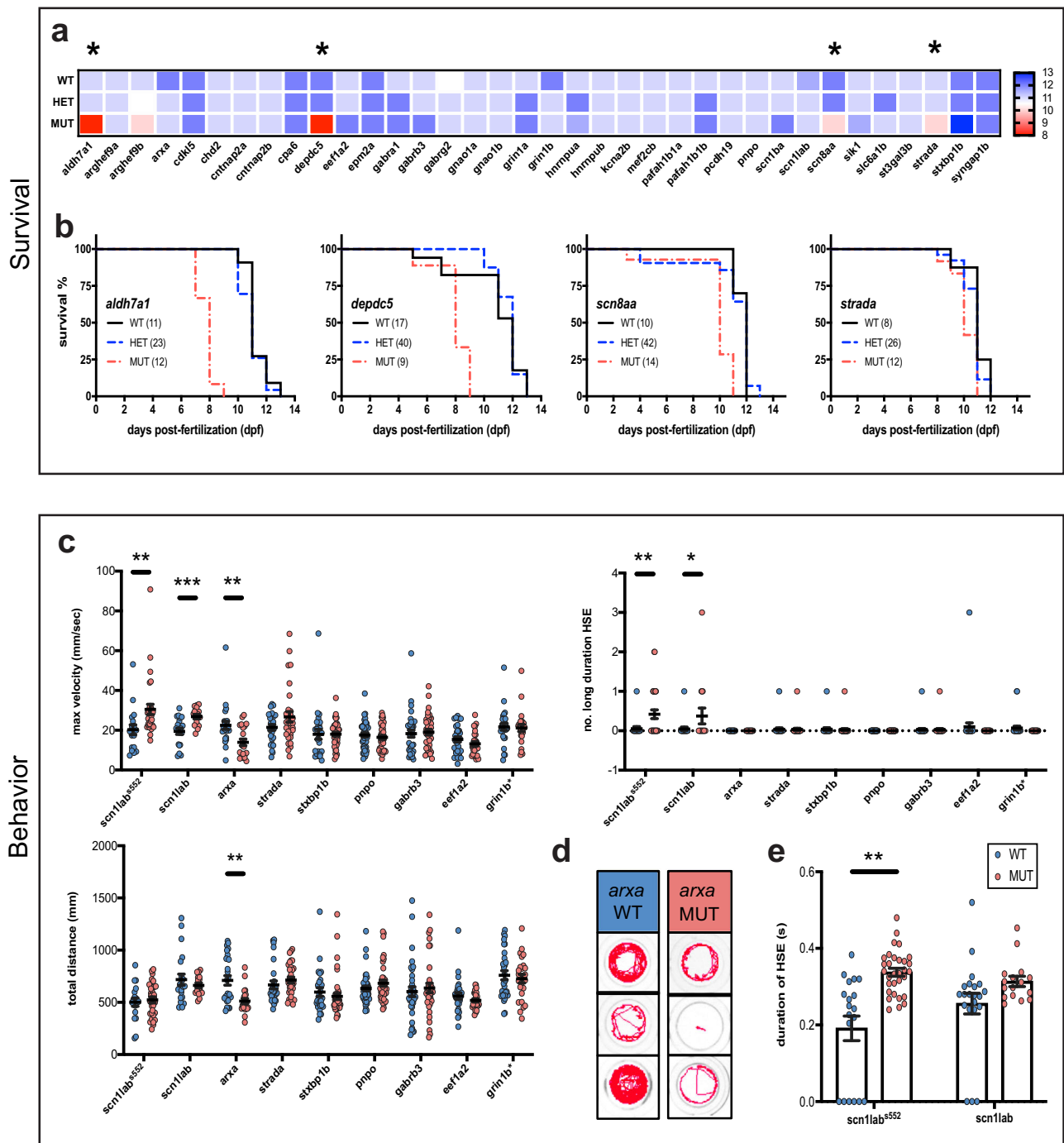
Fig. 6 Survival and behavioral phenotypes. a Heatmap displaying median wild-type (WT), heterozygote (HET), and homozygote mutant (MUT) larval survival for EZP lines. Range extends from 8 dpf (red) to 13 dpf (blue). Asterisks indicate MUTs with significant survival deficits compared WT control siblings; $p < 0.05$, log rank test. **b** Lines with significant survival deficits. **c** Quantification of the basal locomotor activity of epileptic lines after 1 hr habituation in DanioVision chamber. Maximum velocity and total distance traveled were extracted directly from EthoVision XT 11.5 software while the number of events ≥ 28 mm/s, termed high-speed events (HSE), and long duration HSE (≥ 1 s) were scored using a MATLAB algorithm (scn1lab^{552} WT $N = 19$ larvae, MUT $N = 31$ larvae; scn1lab WT $N = 21$ larvae, MUT $N = 16$ larvae; arxa WT $N = 25$ larvae, MUT $N = 22$ larvae; strada WT $N = 27$ larvae, MUT $N = 31$ larvae; stxbp1b WT $N = 26$ larvae, MUT $N = 43$ larvae; pnpo WT $N = 42$ larvae, MUT $N = 40$ larvae; gabrb3 WT $N = 35$ larvae, MUT $N = 36$ larvae; eef1a2 WT $N = 30$ larvae, MUT $N = 27$ larvae and grin1b WT $N = 29$ larvae and HET $N = 57$ larvae). **d** Representative traces of arxa WT and MUT movement. **e** Comparison of duration of HSE in scn1lab ENU and CRISPR larvae. Data displayed as mean ± SEM, one-way ANOVA was used to determine the significance of both HET and MUT behavior for all lines (Supplementary Figure 4). Post hoc Dunnett multiple comparison test, *$p \leq 0.05$, **$p \leq 0.005$, **$p < 0.0001$.
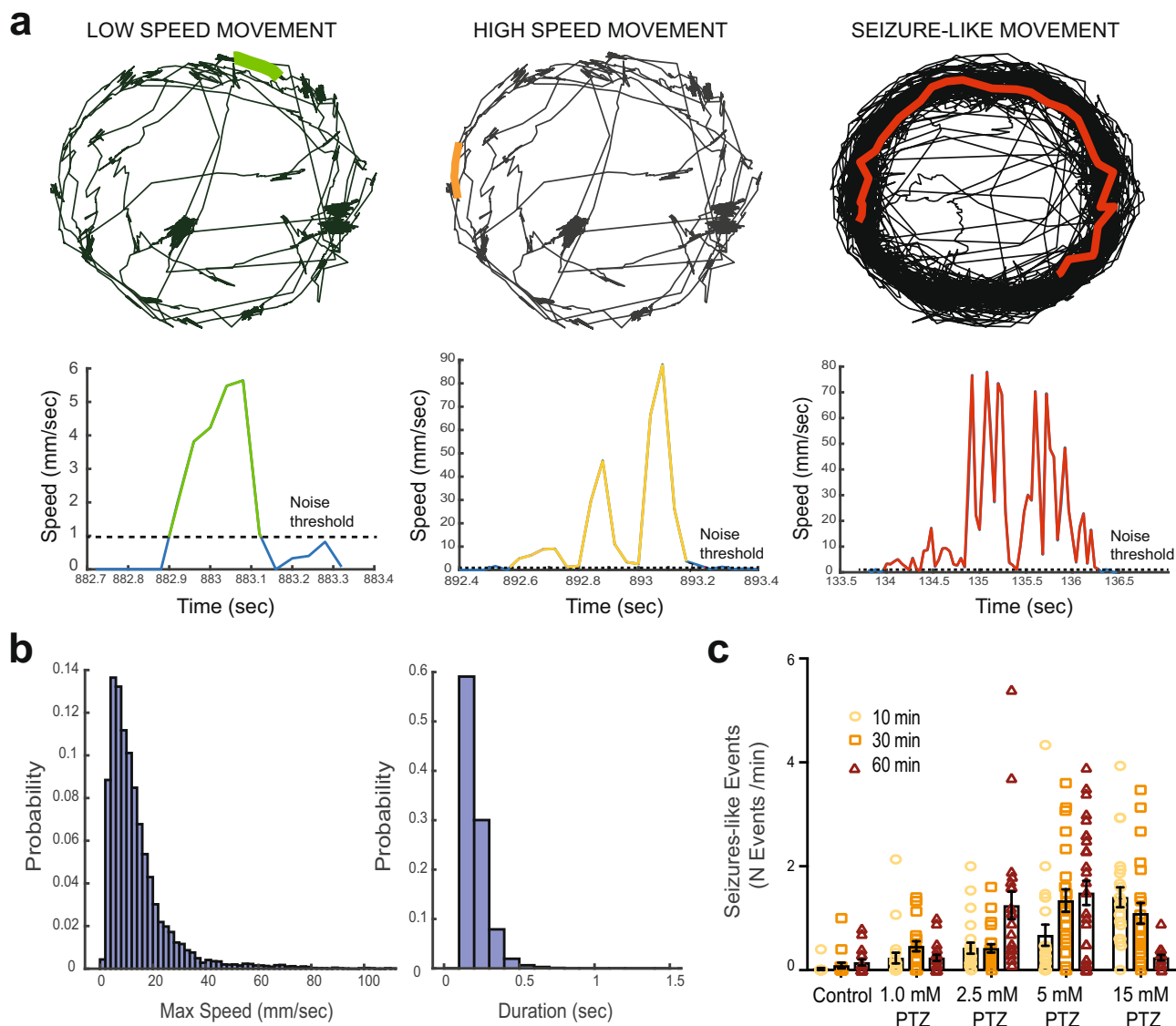
Fig. 7 Automated detection of behavioral seizure-like events. a Example of low-speed movement in a WT larva (green), high-speed movement in the same WT larva (orange), and seizure-like movement in a PTZ-treated larva (red). Top traces represent the larvae track during 15 min recording in a 96-well plate. The bottom panels show speed values across time for the events highlighted. Note the short and long duration in the high-speed events in WT and PTZ-treated larvae, respectively. **b** Distribution of maximum speed and duration across all movements in WT ($N = 109$ larvae) during the 15-minute recording session. The average maximum speed was 10.5 mm/sec and the duration of the events was <1 s. **c** Frequency of seizure-like movements (defined as events with maximum speed >28 mm/sec and duration >1 s) in control and PTZ-treated larvae at different concentrations after 10, 30, and 60 minutes (two-way ANOVA $p < 0.05$). Note the increased number of events with increasing PTZ dose and the lower number when using 15 mM after 60 minutes owing to increased larvae mortality. Data displayed as mean ± SEM.

BX-51W) and monitored continuously using a Zeiss Axiocam digital camera. Under visual guidance, gap-free LFP recordings (15 min duration) were obtained from optic tectum using a single-glass microelectrode (*WPI glass #TW150 F-3*); ~1 µm tip diameter; 2 mM NaCl internal solution), as described[43,44]. LFP voltage signals were low-pass filtered at 1 kHz (−3 dB; eight-pole Bessel), digitized at 10 kHz using a Digidata 1320 A/D interface (Molecular Devices), and stored on a PC computer running AxoScope 10.3 software (Molecular Devices). For pharmacology experiments, continuous gap-free LFP recordings were made for 1 hr and drug concentrations are based on previously published data[23,44]. Larvae were gently freed from agarose at the conclusion of recording epochs for post hoc genotyping by investigators blind to the status of the experiment. Electrophysiology files were also coded for post hoc analysis offline. Experiments were performed on at least three independent clutches of larvae for each line; a minimum of 75 larvae was screened per line. Individual abnormal electrographic seizure-like events were defined as: (i) brief interictal-like events comprised of spike upward or downward membrane deflections >3× baseline noise level or (ii) long duration, large-amplitude ictal-like multi or poly-spike events >5× baseline noise level. Quantification of epileptiform events was performed using Clampfit 10.3 (Molecular Devices) or custom MATLAB (MathWorks; Fig. 3) software by investigators blind

to the status of the experiment. A binning method combined with a sliding window algorithm was used to calculate the active level of the signal within the current time window. The value of each bin was used to identify the start and end of an event. We used a range of voltage thresholds (0.15–0.25 mV, depending on the noise level) and a relative threshold (3× Standard Deviation) for the detection of interictal events. By comparing manual-auto counting results of a testing data sample for each recording (Fig. 4d), we fine-tuned the threshold detection for each recording to a level where auto counting results were close to the manual counting results (<3% difference). All files were uncoded and combined with genotyping data at the end of this process.

Larval behavior

Basal locomotion. Behavioral studies conducted on select EZP lines utilized a 96-well format and automated locomotion detection using a DanioVision system running EthoVision XT 11.5 software (DanioVision, Noldus Information Technology). Zebrafish larvae were transferred from their home incubator to the test room at least 10 min before the experiment. After larvae were individually transferred to wells in ~150 µl of embryo media, the 96-well plate was placed in the
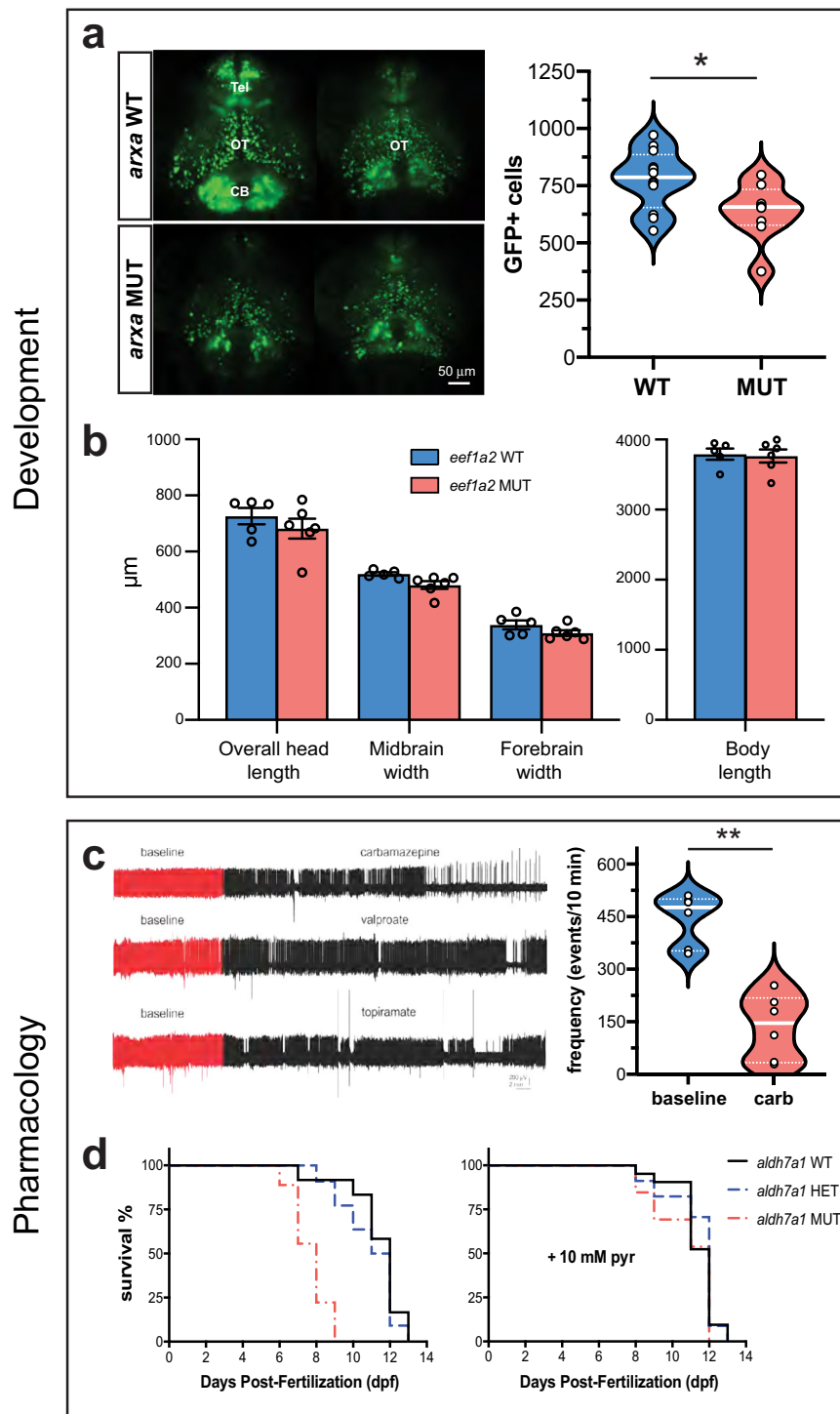
Fig. 8 Developmental and pharmacological characterization. a Representative images of *dlx*-GFP expressing interneurons in *arxa* MUT larvae (*N* = 8) and WT sibling larvae (*N* = 12) obtained from volumetric light-sheet imaging microscopy. Unpaired two-tailed *t* test **p* = 0.0268; *t* = 2.411, *df* = 18). **b** High-resolution images of larvae were taken using a SteREO Discovery.V8 microscope (Zeiss) and overall head length, midbrain width, forebrain width and body length were quantified in *eef1a2* MUT larvae (*N* = 6) and WT sibling larvae (*N* = 5). **c** Representative 1 hr LFP traces from *gabrb3* MUT larvae exposed to AEDs. The first ~10 min of the recording (in red) represents baseline. Drugs were bath applied at a concentration of 0.5 mM; *N* = 3–6 larvae per drug. Results from carbamazepine treatment shown as violin plot. Unpaired two-tailed *t* test ***p* < 0.0001; *t* = 6.344, *df* = 10). **d** Kaplan–Meier survival curves for *aldh7a1* WT, *aldh7a1* HET and *aldh7a1* MUT larvae treatment with 10 mM pyrodixine (pyr) or vehicle for 30 mins daily starting at 4 dpf. Median survival for vehicle-treated *aldh7a1* WT = 12 dpf (*N* = 12), *aldh7a1* HET = 11.5 dpf (*N* = 22 larvae) and *aldh7a1* MUT = 8 dpf (*N* = 9 larvae). Median survival for 10 mM pyridoxine (pyr) treated larvae for *aldh7a1* WT = 12 dpf (*N* = 21 larvae), *aldh7a1* HET = 12 dpf (*N* = 34 larvae) and *aldh7a1* MUT = 12 dpf (*N* = 13 larvae). Data displayed as mean ± SEM.

DanioVision observation chamber and left undisturbed for 1 hr. Larval movement was tracked for 15 min at 25 frames per sec with the following detection settings: method; DanioVision, sensitivity; 110, video pixel smoothing; low, track noise reduction; on, subject contour; 1 pixel (contour dilation, erode first then dilate), subject size; 4-4065. For each zebrafish line, experiments were performed with at least 3 different clutches and post hoc genotyping. The mean and maximum velocity of each larva was calculated. In addition, high-speed seizure behaviors were scored using a MATLAB algorithm developed by our laboratory and validated on PTZ and scn1lab seizure models (Fig. 7).

Seizure-like behavioral events. To classify larval movements, we first processed the videos with EthoVision software 11.5 (Noldus) to identify a larva's position at an acquisition rate of 25 frames/sec, using the same detection settings listed in the "basal locomotion" assay, except with the track noise reduction off. Using custom-written MATLAB-based software, we then extracted movement events defined as times when larvae speed exceeded a threshold of 0.9 mm/sec for at least 160 msec. Adjacent events were combined if the time interval was <40 msec. Furthermore, when the maximum speed within an event was lower or higher than a cutoff threshold, the movement events were classified into low- and high-speed events, respectively. For the analysis in Fig. 7, we calculated the distribution of all movements in a large control group of larvae ($N > 100$) and then identified the speed value threshold at 1.5× standard deviation to be used as a cutoff threshold, unless otherwise specified. Similar results for larval WT movement speeds and duration have been previously reported[76]. Seizure-like events were defined as high-speed movement events that lasted longer than 1 s validated on PTZ and scn1lab seizure models.

Behavioral effects of electrode implantation. WT larvae (5 dpf) in 100 mm petri dishes were transferred to the test room and subjected to one of three treatments:

Treatment 1: Larvae were briefly anesthetized in pancuronium (300 μM) and then immobilized in 2% agarose dorsal side up on a recording chamber. About 3 ml of recording media was added to the chamber then a glass microelectrode was positioned in the forebrain for LFP recording as previously described[43,44]. After 15–30 min, the electrode was removed and the larva gently released from agarose and transferred to a petri dish with embryo medium.

Treatment 2: Larvae were briefly anesthetized in pancuronium (300 μM) and then immobilized in 2% agarose dorsal side up on a recording chamber. After 15–30 min, the larvae were gently released from the agarose and transferred to a petri dish with embryo medium.

Treatment 3: Larvae were left undisturbed in the original petri dish.

At the end of the experiment, all treatment groups were returned to the home incubator until behavioral experiments. Four hours after treatment, larvae were returned to the test room and left undisturbed for 10 min. Larvae were individually transferred to a 96-well plate in ~150 μl of embryo media and the plate then placed in the DanioVision observation chamber. After 15 min, larval movement was tracked for 30 min using settings outlined in "basal locomotion". Once completed, the plate was removed and returned to the home incubator. The same steps were followed to record behavior 24 hr post-treatment.

Survival assay. For each line, 20–24 zebrafish larvae were randomly selected from at least two clutches and were placed in a 100 mm petri dish containing ~40 ml egg water. The larvae were monitored twice daily and dead larvae were lysed using Bioland Zebrafish Quick Lysis Kit. Larvae were left unperturbed throughout the duration of the assay to eliminate potential effects of variations in larval feeding, ultimately providing us with a robust method to identify early-stage larval lethality phenotypes. Unperturbed larvae typically die by 12 dpf[77]. Samples were genotyped using protocols specified in Supplementary Table 3.

Pyridoxine supplementation: aldh7a1 survival. At 4 dpf, larvae were placed individually in 24-well plate with 500 μl 10 mM pyridoxine or egg water (control). Treatment was removed and replaced with fresh egg water. Larvae were then treated with 500 μl 10 mM pyridoxine or egg water (control) for 30 min daily. During daily monitoring, dead larvae were lysed using Bioland Zebrafish Quick Lysis Kit. Samples were genotyped using protocols specified in Supplementary Table 3.

Imaging. For morphology measurements in the *eef1a2* CRISPR line, larvae were placed individually in one well of a μ-well microscope slide (iBidi) and high-resolution images obtained using an optiMOS CMOS camera (QImaging) camera mounted on a SteREO Discovery.V8 stereomicroscope (Zeiss). Files were coded and processed by an investigator blind to status of the experiment. Larvae were collected for independent *post hoc* genotyping at the conclusion of image acquisition. Images were analyzed by a third investigator using DanioScope software (Noldus, version 1.0.109). Standard head (overall head length, midbrain, and forebrain widths) and body length (distance from anterior tip of head to base of caudal fin) measurements were obtained. Files were un-coded and combined with genotyping data at the end of this process.

Interneuron quantification. For imaging studies, *arxa* CRISPR line was crossed with a *dlx5a-dlx6a:GFP:nacre* transgenic zebrafish line provided by Marc Ekker[52]. For analysis of interneuron density in *arxa* WT and homozygote mutants, GFP-expressing larvae were sorted by fluorescence at 2–3 dpf and imaged at 5 dpf using a Zeiss Z.1 light sheet microscope with a ×20 objective. Zebrafish were anesthetized in 0.04% tricaine mesylate and embedded in 2% low melting point agarose inside a glass capillary. The imaging sample chamber was filled with embryo medium. Z-stack images were acquired at 5 μm intervals starting at the first visible dorsal GFP-positive cell. Following image acquisition, larvae were gently removed from agar and independently genotyped. Imaging files were coded and analyzed post hoc by an investigator blind to status of the experiment. Images were then processed in Fiji (ImageJ)[78]. Neurons were quantified with an algorithm modified from "3D watershed technique" (ImageJ macro developed by [Bindokas V, 17-September-2014. Available: https://digital.bsd.uchicago.edu/%5Cimagej_macros.html.]).

Statistics and reproducibility. Statistical tests were performed using MATLAB or GraphPad Prism. One-way analysis of variance with Dunnett's multiple comparison tests or non-parametric *t* tests were used. Data are presented as mean ± S.E.M.

Using mutant (*scn1lab*) and WT control data sets from prior studies, we made a sample-size calculation with a power of 99.9% and $p = 0.001$ to minimize false positives. This analysis determined that a sample size of 16 will be sufficient to detect a 60% effect in mutant larvae relative to WT controls or baseline. Individual analyses and sample sizes are described in Results or Figure legend sections. No data were excluded. All experiments included biological replicates on separate clutches of larvae. All experiments were repeated in triplicate. Larvae used for all experiments were distributed to different behavioral, electrophysiological, or imaging protocols using a block randomization protocol. The block randomization method is designed to randomize subjects into groups that result in equal sample sizes and ensures a balance in a sample size across groups over time. The block size chosen here is based on prior studies and is a multiple of the number of groups, i.e., two experimental groups, WT, and homozygous mutant. We used a total block size of $n = 30$ randomly chosen larvae to obtain a minimum of 6–8 homozygous mutants per experiment.

To eliminate any potential investigator bias, all experiments incorporated (i) blinded conduct as zebrafish caretakers and investigators executing experiments are blinded to the identity of the zebrafish breeding pair and (ii) blinded assessment of outcome as all measurement or quantification of experimental outcomes are performed on coded files by independent investigators. All larvae were independently tested post hoc by extracting DNA from each fish and genotyping the appropriate gene locus. To achieve this level of rigor, laboratory technicians are solely responsible for breeding and maintenance of all zebrafish lines, graduate students, or postdoctoral fellows perform experiments in a blinded manner and code the resulting data files, and finally, a different laboratory technician, graduate student, postdoc, or PI analyzes the coded data files.

Reporting summary. Further information on research design is available in the Nature Research Reporting Summary linked to this article.

Data availability

Representative electrophysiology tracings, Kaplan–Meier survival plots, behavioral data, sequencing information are available on our web-portal (https://zebrafishproject.ucsf.edu). The data sets generated during the current studies are available from the corresponding author on reasonable request.

Code availability

All custom MATLAB programs will be made available upon reasonable request.

References

1. Shields, W. D. Catastrophic epilepsy in childhood. *Epilepsia* **41**, S2–S6 (2000).
2. Camfield, P. & Camfield, C. Epileptic syndromes in childhood: clinical features, outcomes, and treatment. *Epilepsia* **43**, 27–32 (2002).
3. Katsnelson, A., Buzsáki, G. & Swann, J. W. Catastrophic childhood epilepsy: a recent convergence of basic and clinical neuroscience. *Sci. Transl. Med.* **6**, 262ps213 (2014).
4. Pal, D. K., Pong, A. W. & Chung, W. K. Genetic evaluation and counseling for epilepsy. *Nat. Rev. Neurol.* **6**, 445–453 (2010).
5. Myers, C. T. & Mefford, H. C. Advancing epilepsy genetics in the genomic era. *Genome Med.* **7**, 91 (2015).
6. Perucca, P. & Perucca, E. Identifying mutations in epilepsy genes: Impact on treatment selection. *Epilepsy Res.* **152**, 18–30 (2019).

7. Hamdan, F. F. et al. High rate of recurrent de novo mutations in developmental and epileptic encephalopathies. *Am. J. Hum. Genet.* **101**, 664–685 (2017).

8. Epi4K Consortium. et al. De novo mutations in epileptic encephalopathies. *Nature* **501**, 217–221 (2013).

9. Mastrangelo, M. & Leuzzi, V. Genes of early-onset epileptic encephalopathies: from genotype to phenotype. *Pediatr. Neurol.* **46**, 24–31 (2012).

10. Epilepsy Genetics Initiative. The epilepsy genetics initiative: systematic reanalysis of diagnostic exomes increases yield. *Epilepsia* **60**, 797–806 (2018).

11. EpiPM Consortium. A roadmap for precision medicine in the epilepsies. *Lancet Neurol.* **14**, 1219–1228 (2015).

12. Howe, K. et al. The zebrafish reference genome sequence and its relationship to the human genome. *Nature* **496**, 498–503 (2013).

13. Liu, J. et al. CRISPR/Cas9 in zebrafish: an efficient combination for human genetic diseases modeling. *Hum. Genet.* **136**, 1–12 (2017).

14. Adamson, K. I., Sheridan, E. & Grierson, A. J. Use of zebrafish models to investigate rare human disease. *J. Med. Genet.* **55**, 641–649 (2018).

15. Liu, C. X. et al. CRISPR/Cas9-induced shank3b mutant zebrafish display autism-like behaviors. *Mol. Autism* **9**, 23 (2018).

16. Thyme, S. B. et al. Phenotypic landscape of schizophrenia-associated genes defines candidates and their shared functions. *Cell* **177**, 478–491.e420 (2019).

17. Tang, W. et al. Genetic control of collective behavior in zebrafish. *iScience* **23**, 100942 (2020).

18. Vaz, R., Hofmeister, W. & Lindstrand, A. Zebrafish models of neurodevelopmental disorders: limitations and benefits of current tools and techniques. *Int. J. Mol. Sci.* **20**, 1296 (2019).

19. Sakai, C., Ijaz, S. & Hoffman, E. J. Zebrafish models of neurodevelopmental disorders: past, present, and future. *Front. Mol. Neurosci.* **11**, 294 (2018).

20. Gupta, T. et al. Morphometric analysis and neuroanatomical mapping of the zebrafish brain. *Methods* **150**, 49–62 (2018).

21. Khan, K. M. et al. Zebrafish models in neuropsychopharmacology and CNS drug discovery. *Br. J. Pharm.* **174**, 1925–1944 (2017).

22. Cornet, C., Di Donato, V. & Terriente, J. Combining zebrafish and CRISPR/Cas9: toward a more efficient drug discovery pipeline. *Front. Pharm.* **9**, 703 (2018).

23. Baraban, S. C., Dinday, M. T. & Hortopan, G. A. Drug screening in Scn1a zebrafish mutant identifies clemizole as a potential Dravet syndrome treatment. *Nat. Commun.* **4**, 2410 (2013).

24. Griffin, A. et al. Clemizole and modulators of serotonin signalling suppress seizures in Dravet syndrome. *Brain* **140**, 669–683 (2017).

25. Cully, M. Zebrafish earn their drug discovery stripes. *Nat. Rev. Drug Discov.* **18**, 811–813 (2019).

26. Weuring, W. J. et al. NaV1.1 and NaV1.6 selective compounds reduce the behavior phenotype and epileptiform activity in a novel zebrafish model for Dravet Syndrome. *PloS ONE* **15**, e0219106 (2020).

27. Dinday, M. T. & Baraban, S. C. Large-scale phenotype-based antiepileptic drug screening in a zebrafish model of dravet syndrome. *eNeuro* **2**, ENEURO.0068-15.2015 (2015).

28. Thornton, C., Dickson, K. E., Carty, D. R., Ashpole, N. M. & Willett, K. L. Cannabis constituents reduce seizure behavior in chemically-induced and scn1a-mutant zebrafish. *Epilepsy Behav.* **110**, 107152 (2020).

29. Griffin, A., Anvar, M., Hamling, K. & Baraban, S. C. Phenotype-based screening of synthetic cannabinoids in a dravet syndrome zebrafish model. *Front. Pharm.* **11**, 464 (2020).

30. Epilepsy, C. o. C. a. T. o. t. I. L. A. Proposal for revised clinical and electroencephalographic classification of epileptic seizures. from the commission on classification and terminology of the international league against epilepsy. *Epilepsia* **22**, 489–501 (1981).

31. Engel, J. Jr. A proposed diagnostic scheme for people with epileptic seizures and with epilepsy: report of the ILAE task force on classification and terminology. *Epilepsia* **42**, 796–803 (2001).

32. Berg, A. T. et al. Revised terminology and concepts for organization of seizures and epilepsies: report of the ILAE Commission on Classification and Terminology, 2005-2009. *Epilepsia* **51**, 676–685 (2010).

33. Fisher, R. S. et al. Operational classification of seizure types by the international league against epilepsy: position paper of the ilae commission for classification and terminology. *Epilepsia* **58**, 522–530 (2017).

34. Akman, O. et al. Methodologic recommendations and possible interpretations of video-EEG recordings in immature rodents used as experimental controls: a TASK1-WG2 report of the ILAE/AES joint translational task force. *Epilepsia Open* **3**, 437–459 (2018).

35. Grone, B. P. & Baraban, S. C. Animal models in epilepsy research: legacies and new directions. *Nat. Neurosci.* **18**, 339–343 (2015).

36. Wong, M. & Roper, S. N. Genetic animal models of malformations of cortical development and epilepsy. *J. Neurosci. Methods* **260**, 73–82 (2016).

37. Demarest, S. T. & Brooks-Kayal, A. From molecules to medicines: the dawn of targeted therapies for genetic epilepsies. *Nat. Rev. Neurol.* **14**, 735–745 (2018).

38. Yang, Y. & Frankel, W. N. Genetic approaches to studying mouse models of human seizure disorders. *Adv. Exp. Med. Biol.* **548**, 1–11 (2004).

39. Hwang, W. Y. et al. Heritable and precise zebrafish genome editing using a CRISPR-Cas system. *PLoS ONE* **8**, e68708 (2013).

40. Hwang, W. Y. et al. Efficient genome editing in zebrafish using a CRISPR-Cas system. *Nat. Biotechnol.* **31**, 227–229 (2013).

41. Allen, A. S. et al. De novo mutations in epileptic encephalopathies. *Nature* **501**, 217–221 (2013).

42. Grone, B. P. et al. Epilepsy, behavioral abnormalities, and physiological comorbidities in syntaxin-binding protein 1 (STXBP1) mutant zebrafish. *PLoS ONE* **11**, e0151148 (2016).

43. Baraban, S. C. Forebrain electrophysiological recording in larval zebrafish. *J. Vis. Exp.* https://doi.org/10.3791/50104 (2013).

44. Baraban, S. C., Taylor, M. R., Castro, P. A. & Baier, H. Pentylenetetrazole induced changes in zebrafish behavior, neural activity and c-fos expression. *Neuroscience* **131**, 759–768 (2005).

45. Baraban, S. C. et al. A large-scale mutagenesis screen to identify seizure-resistant zebrafish. *Epilepsia* **48**, 1151–1157 (2007).

46. Pena, I. A. et al. Pyridoxine-dependent epilepsy in zebrafish caused by Aldh7a1 deficiency. *Genetics* **207**, 1501–1518 (2017).

47. Hunyadi, B., Siekierska, A., Sourbron, J., Copmans, D. & de Witte, P. A. M. Automated analysis of brain activity for seizure detection in zebrafish models of epilepsy. *J. Neurosci. Methods* **287**, 13–24 (2017).

48. Kedra, M. et al. TrkB hyperactivity contribute to brain dysconnectivity, epileptogenesis, an anxiety in zebrafish model of Tuberous Sclerosis Complllllex. *Proc. Natl Acad. Sci. USA* **117**, 2170–2179 (2020).

49. Kato, M. & Dobyns, W. B. X-linked lissencephaly with abnormal genitalia as a tangential migration disorder causing intractable epilepsy: proposal for a new term, "interneuronopathy". *J. Child Neurol.* **20**, 392–397 (2005).

50. Marsh, E. D. et al. Developmental interneuron subtype deficits after targeted loss of Arx. *BMC Neurosci.* **17**, 35 (2016).

51. Friocourt, G. & Parnavelas, J. G. Mutations in ARX result in several defects involving GABAergic neurons. *Front. Cell Neurosci.* **4**, 4 (2010).

52. Yu, M. et al. Activity of dlx5a/dlx6a regulatory elements during zebrafish GABAergic neuron development. *Int. J. Dev. Neurosci.* **29**, 681–691 (2011).

53. McLachlan, F., Sires, A. M. & Abbott, C. M. The role of translation elongation factor eEF1 subunits in neurodevelopmental disorders. *Hum. Mutat.* **40**, 131–141 (2019).

54. Papandreou, A. et al. GABRB3 mutations: a new and emerging cause of early infantile epileptic encephalopathy. *Dev. Med. Child Neurol.* **58**, 416–420 (2016).

55. Zabinyakov, N. et al. Characterization of the first knock-out aldh7a1 zebrafish model for pyridoxine-dependent epilepsy using CRISPR-Cas9 technology. *PLoS ONE* **12**, e0186645 (2017).

56. Leu, C. et al. Polygenic burden in focal and generalized epilepsies. *Brain* **142**, 3473–3481 (2019).

57. Henshall, D. C. & Kobow, K. Epigenetics and epilepsy. *Cold Spring Harb. Perspect. Med.* **5**, a022731 (2015).

58. Zhang, Y. H. et al. Genetic epilepsy with febrile seizures plus: Refining the spectrum. *Neurology* **89**, 1210–1219 (2017).

59. Amendola, E. et al. Mapping pathological phenotypes in a mouse model of CDKL5 disorder. *PLoS ONE* **9**, e91613 (2014).

60. Wang, I. T. et al. Loss of CDKL5 disrupts kinome profile and event-related potentials leading to autistic-like phenotypes in mice. *Proc. Natl Acad. Sci. USA* **109**, 21516–21521 (2012).

61. Kim, Y. J. et al. Chd2 is necessary for neural circuit development and long-term memory. *Neuron* **100**, 1180–1193.e186 (2018).

62. Yuskaitis, C. J. et al. A mouse model of DEPDC5-related epilepsy: neuronal loss of Depdc5 causes dysplastic and ectopic neurons, increased mTOR signaling, and seizure susceptibility. *Neurobiol. Dis.* **111**, 91–101 (2018).

63. Zaman, T., Abou Tayoun, A. & Goldberg, E. M. A single-center SCN8A-related epilepsy cohort: clinical, genetic, and physiologic characterization. *Ann. Clin. Transl. Neurol.* **6**, 1445–1455 (2019).

64. Kolc, K. L. et al. A systematic review and meta-analysis of 271 PCDH19-variant individuals identifies psychiatric comorbidities, and association of seizure onset and disease severity. *Mol. Psychiatry* **24**, 241–251 (2019).

65. Borlot, F., Whitney, R., Cohn, R. D. & Weiss, S. K. MEF2C-related epilepsy: delineating the phenotypic spectrum from a novel mutation and literature review. *Seizure* **67**, 86–90 (2019).

66. Mirzaa, G. M. et al. CDKL5 and ARX mutations in males with early-onset epilepsy. *Pediatr. Neurol.* **48**, 367–377 (2013).

67. Scheldeman, C. et al. mTOR-related neuropathology in mutant tsc2 zebrafish: phenotypic, transcriptomic and pharmacological analysis. *Neurobiol. Dis.* **108**, 225–237 (2017).

68. Liao, M. et al. Targeted knockout of GABA-A receptor gamma 2 subunit provokes transient light-induced reflex seizures in zebrafish larvae. *Dis. Model. Mech.* **12**, dmm040782 (2019).

69. Fuller, T. D., Westfall, T. A., Das, T., Dawson, D. V. & Slusarski, D. C. High-throughput behavioral assay to investigate seizure sensitivity in zebrafish implicates ZFHX3 in epilepsy. *J. Neurogenet.* **32**, 92–105 (2018).

70. Hoffman, E. J. et al. Estrogens suppress a behavioral phenotype in zebrafish mutants of the autism risk gene, CNTNAP2. *Neuron* **89**, 725–733 (2016).

71. Brueggeman, L. et al. Drug repositioning in epilepsy reveals novel antiseizure candidates. *Ann. Clin. Transl. Neurol.* **6**, 295–309 (2019).

72. Teng, Y. et al. Knockdown of zebrafish Lgi1a results in abnormal development, brain defects and a seizure-like behavioral phenotype. *Hum. Mol. Genet* **19**, 4409–4420 (2010).

73. Samarut, É. et al. γ-Aminobutyric acid receptor alpha 1 subunit loss of function causes genetic generalized epilepsy by impairing inhibitory network neurodevelopment. *Epilepsia* **59**, 2061–2074 (2018).

74. Liu, F. et al. A novel LGI1 missense mutation causes dysfunction in cortical neuronal migration and seizures. *Brain Res.* **1721**, 146332 (2019).

75. Pasquier, J. et al. Gene evolution and gene expression after whole genome duplication in fish: the PhyloFish database. *BMC Genomics* **17**, 368 (2016).

76. Mirat, O., Sternberg, J. R., Severi, K. E. & Wyart, C. ZebraZoom: an automated program for high-throughput behavioral analysis and categorization. *Front. Neural Circuits* **7**, 107 (2013).

77. Lucore, E. C. & Connaughton, V. P. Observational learning and irreversible starvation in first-feeding zebrafish larvae: is it okay to copy from your friends? *Zoology* **145**, 125896 (2021).

78. Schindelin, J. et al. Fiji: an open-source platform for biological-image analysis. *Nat. Methods* **9**, 676–682 (2012).

Acknowledgements

Author contributions

A.G. and S.C.B. conceived the project. A.G. and C.C. designed the CRISPR strategy and trained subsequent personnel on the generation of mutant lines. A.G. and C.C. directed and supervised the research. A.G., C.C., J.L., B.G., and K.H. generated mutant zebrafish lines. A.G., K.H., and M.A. conducted gene expression studies. C.C. designed and guided the behavioral assay studies. C.C. and C.O. collected the behavioral data and C.C., C.O. and R.P. analyzed the behavioral data. S.C.B., M.M., and M.T.D. collected and analyzed electrophysiology data. T.Q. and J.L. collected and analyzed light-sheet microscopy data. C.C., M.M., and F.F. collected and analyzed survival data. J.L. and R.P. designed and wrote MATLAB programs for data analysis. M.M. and C.O. created the database website. M.T.D., M.A., C.O., and F.F. maintained the zebrafish colony. A.G., C.C., and S.C.B. wrote and edited the paper.

Competing interests

The authors declare the following competing interests: S.C.B. is a co-Founder and Scientific Advisor for EpyGenix Therapeutics. S.C.B. is on the Scientific Advisory Board of ZeClinics. The remaining authors declare that the research was conducted in the absence of any commercial or financial relationships that could be construed as a potential conflict of interest.

Additional information

Supplementary information The online version contains supplementary material available at https://doi.org/10.1038/s42003-021-02221-y.

Correspondence and requests for materials should be addressed to S.C.B.

Peer review information *Communications Biology* thanks the anonymous reviewers for their contribution to the peer review of this work.

Reprints and permission information is available at http://www.nature.com/reprints

Publisher's note Springer Nature remains neutral with regard to jurisdictional claims in published maps and institutional affiliations.